Periodico di Mineralogia (2011), 80, 3 (Spec. Issue), 433-453 DOI: 10.2451/2011PM0029

PERIODICO di MINERALOGIA
established in 1930

An International Journal of
MINERALOGY, CRYSTALLOGRAPHY, GEOCHEMISTRY,
ORE DEPOSITS, PETROLOGY, VOLCANOLOGY
and applied topics on *Environment*, *Archeometry* and *Cultural Heritage*

Potential of vis-NIR reflectance spectroscopy for the mineralogical characterization of synthetic gleys: a preliminary investigation

Natalia Leone[1], Mariano Mercurio[1,*], Eleonora Grilli[2], Antonio P. Leone[3], Alessio Langella[1] and Andrea Buondonno[2]

[1] Department of Biological, Geological and Environmental Sciences, University of Sannio, Via dei Mulini 59/A, 82100 Benevento, Italy
[2] Department of Environmental Sciences, Second University of Naples, Via Vivaldi 43, 81100 Caserta, Italy
[3] Italian National Research Council (CNR), Institute for Mediterranean Agriculture and Forest Systems, Via Patacca 85, 80056 Ercolano (NA), Italy
[*]Corresponding author: *mamercur@unisannio.it*

Abstract

An investigation was carried out aiming at assessing the potential of vis-NIR reflectance spectroscopy, through comparison with the conventional X-ray powder diffraction (XRPD) technique, for the characterization of synthetic gleys, obtained in laboratory starting from Fe^0 and Fe^{2+} under different conditions of initial pH (5.5, 7.0 and 8.5). XRPD analysis showed that in any case goethite formed, whereas magnetite and lepidocrocite developed in the less oxidised, and akaganéite and hematite in the more oxidised environments. Magnetite was found only starting from Fe^0, i.e. in the less oxidative condition, whereas sporadic hematite was detected just in Fe^{2+} synthetic gleys at 8.5 pH. Vis-NIR reflectance spectroscopy fully confirmed XRPD results. The features of reflectance spectra allowed (i) to discriminate Fe^{2+} from Fe^0 synthetic gleys; (ii) to detect goethite and akaganéite in the high-reflectance spectra of Fe^{2+} synthetic gleys; (iii) to correlate the very poor reflectance of Fe^0 synthetic gley spectra to magnetite; and, (iv) to identify some goethite and lepidocrocite features in Fe^0 synthetic gleys spectra. The analysis of second-derivative spectra also addressed to goethite, lepidocrocite and magnetite in Fe^0 synthetic gleys; and (ii) goethite, akaganéite and - at pH 8.5 - hematite in Fe^{2+} synthetic gleys. The results obtained appear to be as original as significant, introducing vis-NIR reflectance spectroscopy as an innovative and promising effective method for the characterization of the soil gley forms, and highly stimulating for further investigations.

Key words: vis-NIR spectroscopy; X-Ray Powder Diffraction; soil gley; iron oxides; synthetic gleys.

Introduction

Iron represents one of the most abundant elements of the earth's crust comprising around 5% by mass. As a result of iron's abundance and its close association with biological systems, the chemical transformations and mineralogical phases of iron have played a key role in Earth surface systems (Taylor and Konhauser, 2011). The well-known iron wide variability in oxidation states generates several important minerals belonging to different mineralogical classes such as native or metal forms, silicates, phosphates, sulfides, carbonates and oxides. As far as soils are considered, iron preferentially occurs as oxides in a variety of forms with different crystalline order. Together with manganese, iron is the element that undergoes the most interesting transformations in soil, as a consequence of its geochemical dynamics strongly influenced by changes of redox potential. Such conditions occur in soils with "aquic" (L. *aqua*, water) features, i.e. soils which currently experience continuous or periodic saturation and reduction (USDA-NRCS, 1999). Consequently, "redoximorphic features" (USDA-NRCS, 1999) occur in soil as "redox concentrations", zones of apparent accumulation of Fe-Mn oxides, or "redox depletions", where Fe-Mn oxides alone or both Fe-Mn oxides and clay have been stripped out. Since reduction and oxidation processes are also function of soil pH, variations of soil reaction imply changes in redoximorphic equilibria.

The various forms of the iron redox products take as a whole the name of gley (from Russian, meaning "mucky soil mass", IUSS-ISRIC-FAO, 2006), and the processes forming gleys are termed "gleysation". According to the Soil Science Society of America (2008) a gley soil is a "soil developed under conditions of poor drainage resulting in reduction of iron and other elements and in gray colours and mottle". On the other hand, the WRBSR (IUSS-ISRIC-FAO, 2006) defines "Gleysols" as wetland soils that, unless drained, are saturated with groundwater for long enough periods to develop a characteristic gleyic colour pattern. This pattern is essentially made up of reddish, brownish or yellowish colours at ped surfaces and/or in the upper soil layer or layers, in combination with greyish/bluish colours inside the peds and/or deeper in the soil". Since redox variations in soil are depending on oxic-anoxic fluctuations, the identification of gley formations also is an important indicator of the dynamics of water in the soil.

Gleysation is typical of areas with high annual rainfall and low potential evapotranspiration. However, gleyed soils are also found in Mediterranean climate regions (Torrent, 1995), where poor drainage and/or rising groundwater lead to "aquic" conditions predisposing alternating redox, particularly in landscape depressions, endorheic areas and river valleys.

As above mentioned, reducing conditions induced by permanent wet conditions determine the development of reductimorphic colours, dominated by shades of blue-green iron hydroxides with very low (< 2) colour component chroma. Alternating reducing and oxidising conditions, occurring in soil with fluctuating groundwater, produce oximorphic colours, resulting from the presence of various iron oxides. Consequently, the identification of gley formations is usually carried out in the field, by visually matching the colour of a soil sample with standard Munsell colour charts (Schoeneberger et al., 2002). Although useful for a rapid diagnosis of the variability of the redox dynamics in soils, the Munsell method does not investigate the nature of the different phases of iron that contribute to the expression of the colour itself. On the other hand, conventional laboratory techniques are inapplicable at all to gleys characterizations, since gley formations are ephemeral, often consisting of iron compounds deposited as very thin coatings on the surface of

peds, or of soil pores, and therefore almost impossible to extract and analyse them. Hence, a substantial need exists to investigate the suitability of alternative techniques to achieve accurate information on the composition of gley.

Visible-near infrared (vis-NIR) reflectance spectroscopy, already successfully used for the characterization of various soil features (e.g., organic carbon, clays and clay minerals, iron oxides; Stenberg et al., 2010), could be advantageously used for the identification of gley forms. This technique is based on the investigation of interactions of light with materials in the 350-2500 nm spectral range.

The present paper reports the results of a preliminary study aiming at assessing the potential of vis-NIR reflectance spectroscopy, through comparison with the conventional X-ray powder diffraction (XRPD) technique, for the characterization of synthetic gleys obtained in the laboratory starting from Fe^0 and Fe^{2+} under different conditions of initial pH. In fact, in the light of the considerations above, we thought it appropriate to utilize, as starting materials, both elemental Fe and Fe^{2+} salt, and operate at different pHs. This was done to produce the widest range of initial reaction milieux, with reference to both redox potentials and acidic to alkaline environment, aiming at obtaining the largest differentiation among iron end-products.

Soil Oxides

As previously stated, the oxidative phase of gleysation can produce many different forms of iron oxides, hydroxides and oxi-hydroxides, collectively referred as iron oxides. A brief description of these forms, basically with reference to the works of Cornell and Schwertmann (2003), Scheinost (2004) and Schwertmann (2008) would be useful, in supporting the subsequent discussions. Almost all iron oxides, hydroxides and oxi-hydroxides exist in crystalline form. Their basic structural unit is an octahedron, in which each Fe is surrounded by six O or both O and H ions. Thus, various iron oxides differ mainly in arrangement of the octahedrons. The O and OH ions form either hexagonally close-packed (hcp), or cubic close-packed (ccp) layers. The former represent the α phases, the latter the γ phases. The octahedrons may be linked by corners, edges or faces or combinations of these linkages to form different structural arrays (Figure 1).

Goethite (α-FeOOH) along with hematite (α-Fe_2O_3) is by far the most common iron oxide in soils. This is partially due to its thermodynamic stability, as attested by its low solubility. Its formation is favoured by slow hydrolysis of Fe^{3+} hydroxy cations at low temperature. Therefore, an even distribution of goethite in a soil horizon suggests a pedogenesis under aerated, temperate, humid conditions. The crystal structure of goethite consists in double chains of edge-shared octahedra (Figure 1) that are joined to other double chains by sharing corners and by hydrogen bonds.

Hematite forms by dehydroxylation of ferrihydrite. The formation of hematite is favoured by neutral pH, increasing soil temperature, and decreasing water activity. The crystal structure of hematite consists of sheets of edge-shared octahedra. The sheets are connected by edge- and face-sharing octahedrons (Figure 1).

Ferrihydrite (Fe_5HO_8*$4H_2O$) is a poorly crystalline hydrous oxide commonly occurring, in addition to goethite, in soils of temperate - cool climates. It is found in concretions, oxidation horizons of gleyed soils, Fe-enriched B horizons of Spodosols, especially as organo-mineral complexes, and in drains and ditches of lowland soils (Yli-Halla et al., 2006; Vodyanitskii, 2010). It usually forms when soil solution enriched by soluble Fe^{2+} is aerated relatively quickly, or occurs in the presence of compounds with a high affinity for the iron oxide surface, for example organic matter, phosphate and silicate, which inhibit the formation of the

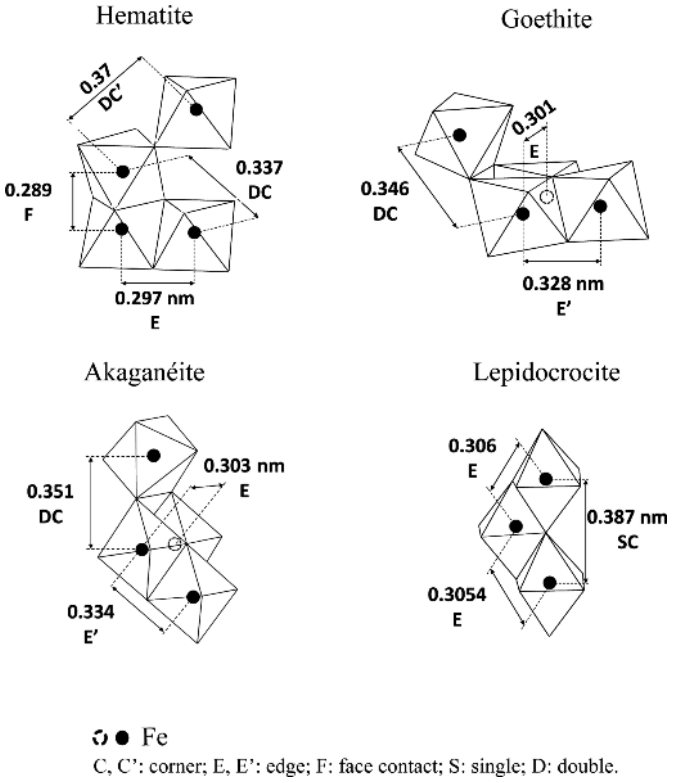

Figure 1. Basic structural units and Fe-Fe distances for hematite, goethite, akaganéite and lepidocrocite (reproduced from Manceau and Drits, 1993).

higher crystalline FeOOH forms.

Lepidocrocite (γ-FeOOH) forms in soils through the oxidation of dissolved Fe^{2+}. However, if the concentration of bicarbonate ions HCO_3^- in solution is substantial, as in neutral-subalkaline soils, calcareous soils or around respiring roots, goethite rather than lepidocrocite will be the oxidation product. Its crystal structure contains double chains of octahedra (Figure 1), which are joined by shared edges, resulting in corrugated sheets of octahedra.

Magnetite (Fe_3O_4) is usually inherited from the parent material, but it may also form in soil through biotic processes. Magnetite can oxidize to maghemite or to hematite. Maghemite (γ-Fe_2O_3) is common in soils of tropical and subtropical climate. Both magnetite and maghemite have the same inverse spinel structure, with octahedral and mixed tetrahedral/octahedral layers stacked along the [111] axis.

Several other iron oxides have rarely or never been observed in soils. They may form in extreme natural environments, as, for instance, akaganéite (β-FeOOHCl). This iron oxide has been found in environments with high chloride concentrations, low pH, and high temperature. Akaganéite consists of 2x2 channels built by edge-sharing double chains (Figure 1). These tunnels contain Cl^- ions that stabilise the structure.

Reflectance spectroscopy: a short review with emphasis on Fe phases

In soils, as well as in rocks, the interaction of light with electromagnetic radiation primarily involves vibrational and electronic transitions (Irons et al., 1989).

The vibrational transitions consist of oscillations in the relative position of bonded atomic nuclei. The oscillations stretch molecular bond lengths and/or bend interbond angles. Transitions in vibrational energy states are generally associated with the absorption of radiation within the infrared portion of the spectrum. In this part of the spectrum, the most important vibrational transitions are those associated with the presence of OH^- ions or water molecules bound in the structure of minerals or present in fluid inclusions (Drury, 1993).

Bands associated with OH^- and H_2O in the NIR are due to the transition of one vibrational mode from a ground state to an energy level two or more levels above the ground state (overtone bands) or to the splitting of an absorbed quantum of radiation to raise energy of more than one vibrational mode (combination bands), while sharper and stronger "fundamental" bands occur in the thermal infrared, between 2500 and 7000 nm (Iron et al., 1989).

Similar vibrational transitions and overtones, which derive from stretching and bending of the C-O bond in the CO_3^{2-} ion, characterize carbonates (Clark et al., 1990; Drury, 1993).

The interaction of light with soil materials also includes transitions in the energy levels of the electrons in soil atoms and molecules. Electronic transitions may be due to charge-transfer modes and crystal field effects. A charge transfer, or inter-element transition, occurs when the absorption of a photon causes an electron to move between ions or between ions and ligands. The transition can also occur between the same metal in different valence state, such as between Fe^{2+} and Fe^{3+}. Crystal field effects are due to unfilled electron shells of transition elements. For all these elements, "d" orbitals have identical energies in an isolated ion, but the energy levels split when the atom is located in a crystal field. This splitting of the orbital energy states enables an electron to be moved from a lower level to a higher one by absorption of a photon having an energy matching the energy difference between the states (Clark, 1999). Electronic transitions generally involve higher energy than vibrational transitions. Thus the absorption of radiation due to the electronic transitions usually occurs at lower wavelengths (i.e. ultraviolet and visible portion of the spectrum), being the level of energy inversely proportional to the wavelength (Iron et al., 1989). The absorption bands associated with electronic transitions involve mainly iron, and are typically much broader than bands corresponding to vibrational transitions (Hunt and Salisbury, 1970).

Spectral reflectance measurements

The spectral reflectance of a sample can be easily derived in the laboratory, using a spectrophotometer, with the help of an integrating sphere and a calibrated white standard (Wyszecki and Stiles, 1982; Escadafal, 1994; Leone and Escadafal, 2001). Laboratory measurements with spectrophotometers offer the prospect of increased precision and have been used successfully for soils (Milton et al., 1995). Nevertheless, they deal only with fine-grained fractions of small soil samples and are very time-consuming in terms of sample collection, preparation and scanning. A considerable number of new instruments, i.e. the spectroradiometers, for field and laboratory spectrometry have emerged in the 1980s. These instruments allow spectra to be recorded in a few seconds over large (from a few square centimetres to several square meters) and undisturbed surfaces. They also allow the acquisition of high-resolution (i.e. better than 5 nm) radiance measurements over the complete reflective spectrum (400 - 2500 nm).

Interpretation of reflectance spectra

Reflectance spectra of samples with unknown mineralogy may simply be interpreted by comparison with spectra of reference minerals (Singer, 1982; Morris et al., 1989). However, the interpretation can be improved after parameterisation of these spectra. Parameterisation is also used for quantitative approaches (Torrent and Barrón, 1993; Leone, 2000; Shepherd and Walsh, 2006; Stenberg et al., 2010). The most frequently used procedures for the parameterisation are: colour calculation (Scheinost and Schwertmann, 1999) and derivative spectroscopy (Scheinost et al., 1998).

Colour calculation

A reflectance spectrum can be converted into a colour by using the basic concepts underlying the perception of this attribute by the human eye (Torrent and Barrón, 2002). In essence the human eye sees colour as a combination of three stimuli, which can be described by corresponding spectral curves, i.e. the colour-matching functions (Cornell and Schwertmann, 1996). A colour stimulus is the radiant energy of given intensity and spectral composition entering the eye and producing a sensation of colour (Judd and Wyszecki, 1975). The colour-matching functions were defined by the Commission Internationale de l'Eclairage (CIE, 1978) for the so-called standard observer. The colour of an object is described by integrating the spectral reflectance and each of the colour matching functions, to obtain the *tristimulus* values X, Y, and Z. These are converted into the chromaticity x and y ($y = x/(X+Y+Z)$; $y = Y/(X+Y+Z)$. In a spectral graph with x and y as axes, the spectral colours form a horse-shoe curve (not shown) enclosing a colour stimuli.

Although the CIE colour scale provides accurate values for colour stimuli, the distance between two colours is poorly correlated with that which the human eye sees. Colour scales have, therefore, been produced (Wyszecki and Stile, 1982) and of these, the CIE 1976 L*a*b* space (CIE, 1978) is widely used.

Figure 2 clarifies such a system. L* represents lightness (0 = black, 100 = white), and a* and b* the chromaticity (+a* = red; -a* = green; +b* = yellow; -b* = blue). Their defining equations are:

$$L^* = 116\,(Y/Y_0)^{1/3} - 16$$

$$a^* = 500\,[(X/X_0)^{1/3} - Y/Y_0)^{1/3}]$$

$$b^* = 200\,[(Y/Y_0)^{1/3} - Z/Z_0)^{1/3}]$$

where X, Y, and Z are the *tristimulus* values of the samples, and X_0, Y_0 and Z_0 are the *tristimulus* value of a reference white.

The specification formed by L*, a*, b* can be transformed into a more intuitive expression, which resembles the Munsell system (see below), using the polar coordinates of the CIE-Lab space L*h*c*. These coordinates correlate well with the perceived value, hue and chroma, respectively. Chroma c* and hue-angle h* are defined as:

$$c^* = (a^{*2} + b^{*2})^{1/2}$$

$$h^* = \arctan\,(b^*/a^*)$$

In soil and other geosciences, colour is commonly measured using the Munsell colour classification system. This system defines colours in terms of hue "H", chroma "C", and value "V" (Escadafal, 1993). Hue refers to the dominant wavelength, and the full series of hues forms a circle. Grey colours, which have no specific hue, form the axis of the cylinder. Chroma expresses the saturation of a colour, and it increases from the centre (chroma = 0) to the periphery of the cylinder, locus of the pure colours (maximum chroma). Value is the overall brightness; the grey axis is defined by values ranging from 0 (black) to 10 (white).

Munsell HVC coordinates can be computed

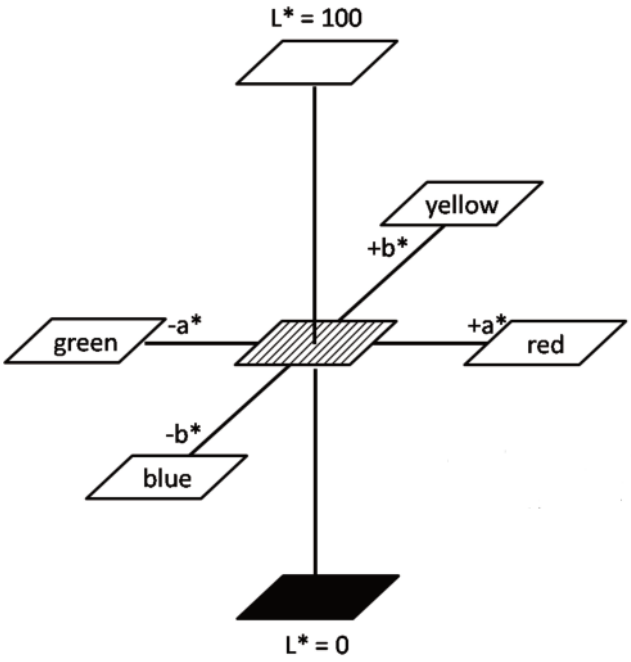

Figure 2. L*a*b* chromaticity colour space.

from the CIE XYZ values by using complex algorithms (Miyahara and Yoshoba, 1988; Viscarra-Rossel et al., 2006).

Colour of iron oxides

Each individual Fe oxide exhibits a colour that is mainly a function of the electron transitions allowed by its structure. Other factors significantly affecting colour include particle size and shape, crystal defects, absorbed impurities, and degree of particle packing. As reported by Torrent and Barrón (2002), particle size is the primary source of colour differences in the same material. This difference can be dramatic in iron oxides: a reduction in particle size of iron oxides results in paler colours; one exception is goethite (Scheinost and Schwertmann, 1999). Aggregation and cementation of individual particles are known to influence colour of many natural iron oxides in a way generally similar to that of an increase in particle size (Torrent and Schwertmann, 1987). The colour of most iron oxides is highly sensitive to crystal impurity and defects. Thus, Al-for-Fe substitutions result in an increase in hematite lightness (Barrón and Torrent, 1984) and chroma (Kosmas et al., 1986), and also in the redness of goethite (Kosmas et al., 1984).

Scheinost et al. (1998) report the mean values and range of variation of the Munsell colour notation of 165 synthetic samples of iron oxides (Table 1).

Hematite has the most reddish average hue, while ferrihydrite, akaganéite, lepidocrocite, maghemite and goethite exhibit hues that are increasingly more yellow. On the other hand, hematite is redder due to the face-sharing octahedral, where adjacent Fe centres are close together as 0.29 nm, thus strongly enhancing ETP

Table 1. Munsell colours of the Fe oxides and hydroxides (median, minimum - maximum).

	Hue	Value	Chroma	Colour name**
Hematite	1.2 YR (3.5R – 4.1YR)	3.6 (2.4 – 4.4)	5.2 (1.5 – 7.9)	Moderate reddish-brown
Goethite	0.4Y (7.3YR – 1.6Y)	6.0 (4.0 – 6.8)	6.9 (6.0 -7.9)	Strong yellowish-brown
Lepidocrocite	6.8YR (4.9YR – 7.9YR)	5.5 (4.6 – 5.9)	8.2 (7.1 – 9.9)	Moderate orange
Ferrihydrite	6.6YR (2.8YR – 9.2YR)	4.9 (2.3 – 6.3)	6.3 (1.9 – 7.3)	Strong brown
Akaganéite	5.5YR (1.2YR – 6.8YR)	3.8 (2.8 – 4.3)	5.8 (4.4 – 7.3)	Strong brown
Magnetite*	(6.5YR – 9.5YR)			Dark yellowish-brown
Maghemite	8.3YR (6.2YR – 9.4YR)	3.1 (2.5 – 3.6)	3.2 (2.5 – 4.1)	Black

* after Scheinost (2004); ** median colour.

(electron pair transition). In contrast, the other minerals are only built up from edge- and corner-sharing octahedral, where Fe centre are 0.30 - 0.33 and 0.35 nm apart, respectively, giving rise to more yellowish hues. Maghemite, and partly oxidised maghemite, have the darkest values due to the co-existence of Fe^{2+} and Fe^{3+} causing IVCT (intervalence charge transfer). The average values of the other, pure Fe^{3+} minerals rank according to their average hues. This ranking reflects the fact that red hues appear darker to the eye than yellow hues. The darker values of maghemite, hematite, akaganéite and ferrihydrite correspond also to their lower chroma.

As stressed by Scheinost (2000), in spite of a substantial variability of colour within the minerals, goethite, hematite, lepidocrocite, and ferrihydrite can be easily distinguished by hue and chroma. Hematite is always redder than 4.1 YR, and goethite is yellower than 7.3 YR. Ferrihydrite and lepidocrocite have intermediate hues, and are separated by chroma. The colour of maghemite is unique due to values lower than 3.6 and hues yellower than 6.2 YR. Akaganéite overlaps with ferrihydrite in hue, value and chroma. Only akaganéite samples with a hue yellower than 5.5 YR may be reliably distinguished from ferrihydrite.

Derivative spectroscopy

Reflectance spectra (R) result from the superposition of absorption bands at different wavelengths, corresponding, as previously stated, to the various electronic or vibrational transitions in the atoms and molecules of minerals. These bands can be enhanced by plotting the second derivative of absorbance (A = log 1/R) against wavelength (Kosmas et al, 1984; Malengreau et al., 1994). The position of an absorption band is indicated by the minimum on the second derivative curve (Huguenin and Jones, 1986), while its amplitude is determined by the difference in ordinate between the minimum and the following maximum. The key feature of second derivative curves is illustrated in Figure 3 for one of the samples used in this study.

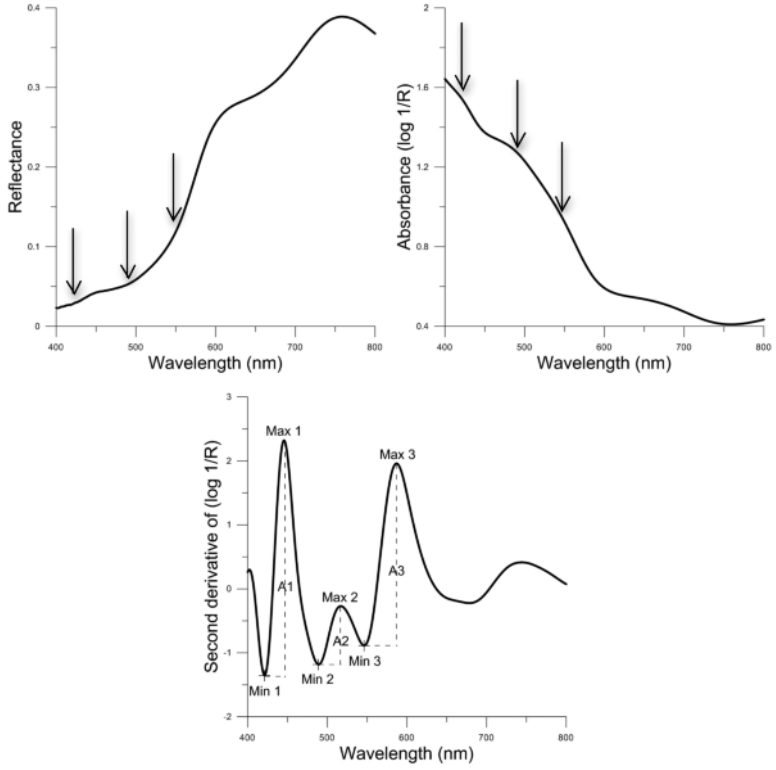

Figure 3. The weak absorption bands in the reflectance curve (top left) become strong minima in the second derivative (bottom) of absorption curve (top right). The amplitude of absorption bands (A1, A2, A3) in the second derivative curve is shown.

Derivative spectroscopy applied to iron oxides

Scheinost et al. (1998) examined the second derivative spectra of 176 synthetic and natural fine-sized, single mineral samples of different iron oxides. The second-derivative spectra of these minerals revealed 4 bands in the range from 350 to 1050 nm. These bands were assigned, according to Sherman and Waite (1985), to the 3 single-electron transitions $^4T_1 \leftarrow ^6A_1$, $^4T_2 \leftarrow ^6A_1$, and (^4E; $^4A_1$) $\leftarrow ^6A_1$, and the electron pair transition (EPT) ($^4T_1$+$^4T_1$) $\leftarrow$ ($^6A_1$+$^6A_1$).

The EPT, as the most intense absorption band, determines the position of the absorption edge which, in turn, is closely related to the hue. The EPTs for hematites occur at 521 to 565 nm, clearly separated from the EPTs of other more yellowish iron oxides (479 to 499 nm). The difference in EPT and colour between hematite and the other iron oxides has been explained by the presence of face-sharing octahedra in the hematite structure leading to an increase of the magnetic coupling between neighbouring Fe^{3+} centres (Sherman and Waite, 1985). In contrast to the results of Malengreau et al. (1994), however, the ranges of the EPT of all other iron oxides generally overlapped, that is, the discrimination of these iron oxides could not be performed with the EPT only.

A similar separation of hematite from the other

iron oxides is given by the $^4T_2 \leftarrow ^6A_1$ transition.

The significantly lower wavelength of this transition for hematite (848-906 nm) is the result of the lower crystal field splitting energy of hematite as compared to that of goethite, maghemite and lepidocrocite (Burns, 1993). Again, strongly overlapping band positions prevents a proper discrimination of the non-hematite iron oxides by only considering this band.

With the $^4T_2 \leftarrow ^6A_1$ transition from 698 to 734 nm, the ferrihydrite samples are distinct from the other iron oxides, where this transition occurs at lower wavelengths (648 to 695 nm). Sixteen out of 22 ferrihydrite samples did not show, however, a second-derivative minimum, so that the band position could not be determined. The $(^4E; ^4A_1) \leftarrow ^6A_1$ transition of iron oxides ranges from 386 to 442 nm. This band was not visible in the derivative spectra of 25 hematites.

Materials and methods

Preparation and separation of synthetic gleys

The present study has been carried out using synthetic gley samples obtained from six different starting solutions/suspensions containing Fe^0 or Fe^{2+}, at pH, 5.5, 7.0 and 8.5, as paradigmatic values of physiological soil reaction range. By this way, we sought to obtain various representative environments of gley formation, different enough to allow the formation of distinct iron-end products.

Elementary iron (Sigma-Aldrich, 99.5% RT) or ferrous chloride tetra-hydrous (Sigma-Aldrich, 99.0% RP) were dissolved in PET beakers by using hydrochloric acid (1:1) or bi-distilled water, respectively. The pH of the resulting iron solutions was then carefully adjusted drop by drop with a solution of NaOH 1N to obtain suspensions nominally containing Fe^0 or Fe^{2+} with initial pH values equal to 5.5, 7.0 and 8.5.

The suspensions were placed in stoppered PET bottles, shaken discontinuously for 7 days, and then stored in a temperature-controlled chamber at 25 °C. After 12 months ageing, the materials were dialysed, then washed with water:acetone 1:1 v/v, oven dried at 40 °C, and ground to pass a 0.5 ∅ mm sieve prior to be analysed.

In every preparation/analysis step, PET vessels were used to avoid any interference by Si of glass labware. For each synthetic gley, up to four subsamples - indicated as a, b, c, or d - have been analysed, according to the observed intrinsic heterogeneity of the mother synthetic gleys themselves.

X-Ray Powder Diffraction (XRPD)

All samples obtained from Fe^0 and Fe^{2+} synthetic gleys were investigated by X-ray powder diffraction (XRPD) using a Philips PW1820 diffractometer (CuKα radiation, 40 kV, 30 mA, 4-50° 2θ scanning interval, 30 s per step counting time, curved graphite monochromator) equipped with Panalytical X-Pert Data Collector and X-Pert HighScore Plus software. Powders with grain size < 10 μm were obtained using a McCrone micronising mill (agate cylinders and wet grinding time 15 min). The investigation allowed the gathering of semi-quantitative data of the occurring phases.

Spectral reflectance measurements

The diffuse vis-NIR reflectance of oven-dried (40 °C) and gently ground samples was measured in the laboratory, under artificial light, using a FieldSpec Pro spectroradiometer (Analytical Spectral Devices). This instrument combines three spectrometers to cover the portion of the spectrum between 350 and 2500 nm. The instrument has a spectral sampling distance of ≤ 1.5 nm for the 350-1000 nm region and 2 nm for the 1000-2500 nm region. The spectrometer optic was mounted at a height of 10 cm, so that the measurement spot size was 4.5 cm in diameter. Each sample was placed inside a circular black capsule of 5 cm in diameter and

0.5 cm depth and levelled with the edge of a spatula to obtain a smooth surface. Soil samples were illuminated with two 100 W halogen lamps, positioned in the same plane, under a 30 degree illumination angle. Measurements were made at the nadir. Radiances were converted to spectral reflectance by dividing the radiance reflected by the target (synthetic gley samples) by that of a standard white reference plate ('spectralon') measured under the same illumination conditions. To reduce instrumental noise, four measurements for each sample were averaged.

Spectral data processing

For each of the average reflectance spectra (hereinafter referred to simply as reflectance spectra) were calculated the *tristimulus* values X, Y and Z, using the software SpecPro (Calabrò and Tosca, 2009). The *tristimulus* values were then converted to Munsell notations and CIE L*a*b* values by using the software Munsell Conversion (http\\walkillcolor.com, 2010). The a* and b* CIE coordinates were then transformed into the c* and h* polar coordinates.

Using SpecPro (Calabrò and Tosca, 2009), reflectance spectra (R) were transformed into absorbance spectra (A = log 1/R) and into second derivative curves. Derivative transformation is particularly sensitive to high frequency instrumental noise, which usually occurs in reflectance spectra. If suitable filtering procedures to suppress this noise are not taken, the signal-to-noise ratio will decrease with increasing derivative order and also with the bandwidth of the signal peak (Chadburn, 1982; O'Havers, 1982; Tsai and Philpot, 1998). Various filtering procedures can be applied to the original spectra or, directly, to the derivative curves (e.g., O'Havers and Green, 1976; Kosmas et al., 1986) to suppress or reduce noise.

One of the most widely used algorithms for this purpose is that of Savitzky and Golay (Savitzky and Golay, 1964), which is based on the fitting a polynomial curve to a set of contiguous data points (usually from 13 to 31) by the least-squares method and calculating the ordinate at the central value of the abscissa (wavelength). A new polynomial curve is then obtained by moving the set one point and calculating the new ordinate. The derivative is obtained by calculating the slope at the central value of the abscissa. The number of points in each set is a crucial input parameter in this procedure. Goodness of fit increases, but degree of smoothing decreases (and resolution increases) with the decreasing number of points, so a compromise must be adopted.

In the present study we applied the Savitzky-Golay filtering to the original spectra, before their transformation into absorbance spectra and the latter into their second derivative curves.

The position of absorption bands determined and their amplitudes calculated, with the help of the software SPEX (Spectral Explorer; Loercher, 1996).

Results and discussion

XRPD mineralogical analysis

Table 2 reports the results of the XRPD obtained for the two sets of investigated Fe^0 or Fe^{2+} synthetic gleys at different pHs 5.5, 7.0, or 8.5. Fe^0 samples are prevailingly characterized by magnetite and goethite and subordinately by lepidocrocite. Halite traces in most of these samples also occur. Magnetite is always the most abundant phase (except for a sample at pH 7.0) and definitely prevails in samples with the lowest pH value 5.5. Goethite also shows different values as a function of the pH with the lowest at 5.5 pH and the highest at 7.0 pH. Lepidocrocite is ubiquitous but in scarce amount.

As far as Fe^{2+} samples are considered it should be remarked the total lack of magnetite and lepidocrocite, while goethite is the most abundant phase along with akaganéite in substantially similar amounts. The only exception was recorded for the sample at the highest pH (8.5) which evidenced also the

Table 2. XRPD mineralogical data concerning samples obtained from Fe^0 and Fe^{2+} synthetic gleys at different pHs.

Synthetic gleys (Sample)	*Fe oxide minerals*					
	Magnetite	Goethite	Lepidocrocite	Hematite	Akaganéite	Halite
Fe^0 pH 5.5 (a)	xxxx	x	x			tr
Fe^0 pH 5.5 (b)	xxxx	x	x			tr
Fe^0 pH 5.5 (c)	xxxx	x	x			
Fe^0 pH 7.0 (a)	xxx	xx	x			
Fe^0 pH 7.0 (b)	xx	xxx	x			
Fe^0 pH 8.5 (a)	xxx	xx	x			tr
Fe^0 pH 8.5 (b)	xxx	xx	x			tr
Fe^0 pH 8.5 (c)	xxx	xx	x			tr
Fe^{2+} pH 5.5		xxx			xx	tr
Fe^{2+} pH 7.0 (a)		xx			xxx	tr
Fe^{2+} pH 7.0 (b)		xx			xxx	
Fe^{2+} pH 7.0 (c)		xx			xxx	tr
Fe^{2+} pH 7.0 (d)		xxx			xx	
Fe^{2+} pH 8.5		xxx		x	xx	tr

a, b, c, d: subsamples; xxxx = very abundant, xxx = abundant, xx = frequent, x = scarce, tr = traces.

presence of hematite. Again, halite was recorded in almost all the samples in a very small amount. Such residual traces clearly are a side-outcome reaction of Na^+ with Cl^- when the suspension acidity was variously neutralised during pH adjusting (see *Preparation and separation of synthetic gleys*, above). Both sets of synthetic gleys (Fe^0 and Fe^{2+}) likely achieved a complete or almost complete crystallisation as revealed by XRPD patterns.

Vis-NIR reflectance spectroscopy

The original reflectance spectra, the soil colour parameters and second derivative spectra were analysed to extract qualitative information on the synthetic gleys being studied.

Visual analysis of reflectance spectra

The visual analysis of reflectance spectra of synthetic gleys was carried out considering three main features: a) the overall reflectance in the whole vis-NIR spectral domain, b) the slope of reflectance spectra in the visible range, c) the presence and intensity of absorption bands (Hunt and Salisbury, 1970; Valeriano et al., 1995).

The comparison between the reflectance spectra of the Fe^0 and Fe^{2+} synthetic gleys (Figure 4) highlights several evident differences in terms of overall reflectance, which is very low (maximum reflectance values < 0.1) in the spectra of Fe^0 synthetic gleys and relatively high in those of the Fe^{2+} synthetic gleys (maximum reflectance value > 0.6).

The comparison between the Fe synthetic gleys, object of the present study, (Figures 4, 6, 7) and those representative of the main iron oxides extracted from a spectral data-library of the United States Geological Survey (USGS; Grove et al., 1992; Figure 5), allows us a first

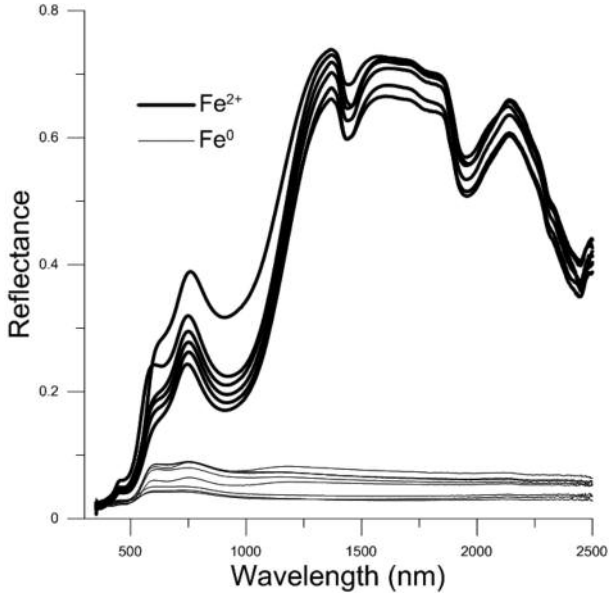

Figure 4. Reflectance spectra of samples of the Fe^0 and Fe^{2+} synthetic gleys.

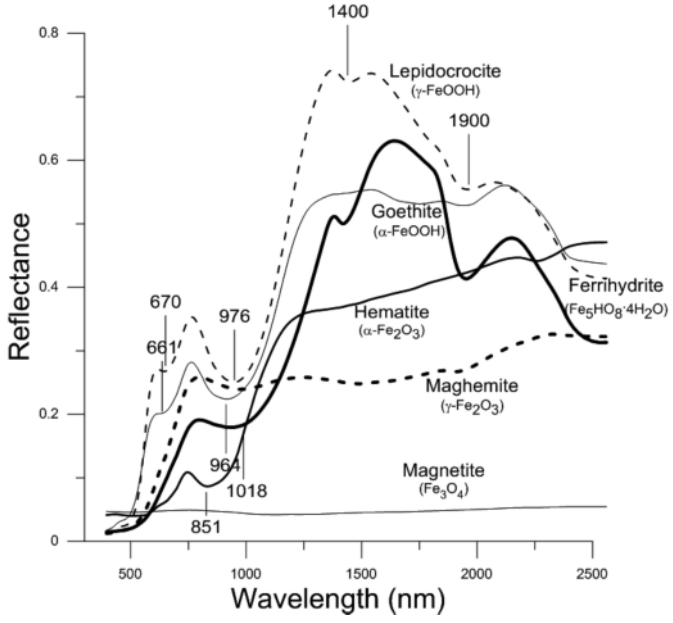

Figure 5. Reflectance spectra of the main soil Fe oxides. Spectra have been extracted from a spectral library of the USGS (United State Geological Survey; Grove et al., 1992) and reprocessed.

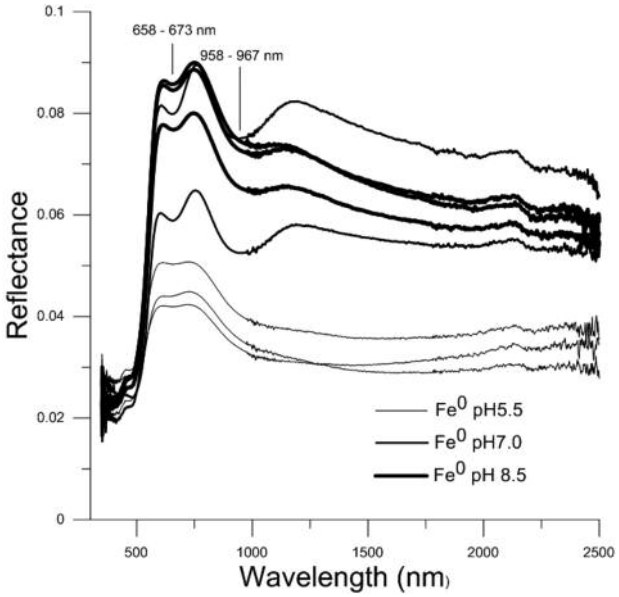

Figure 6. Reflectance spectra of samples of the Fe^0 synthetic gleys. Note that the high signal to noise ratio that appears are due to the very low overall reflectance of spectra.

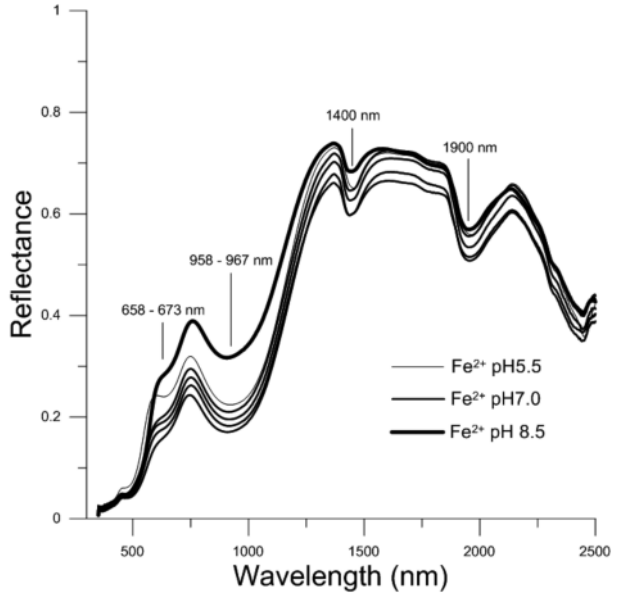

Figure 7. Reflectance spectra of samples of the Fe^{2+} synthetic gleys.

diagnosis of the forms of iron present in the above synthetic gleys.

The high reflectance of the Fe^{2+} synthetic gleys (Figures 4 and 7) may be associated to the presence of lepidocrocite, goethite and ferrihydrite (Figure 5). It must be observed that also the spectra of akaganéite - not plotted because unavailable in digital format in the USGS spectral library - shows a high overall reflectance (Murad and Bishop, 2000).

The low overall reflectance of the Fe^0 synthetic gleys (Figures 4 and 6) is likely due to the presence of magnetite (Figure 5).

Both the Fe^0 and Fe^{2+} synthetic gleys show a step decrease in reflectance in the visible range, toward the blue and ultraviolet wavelengths, due to a strong iron-oxygen charge transfer band that extends into the ultraviolet (Hunt, 1980).

The Fe^{2+} synthetic gleys (Figure 7) display several sharp bands in the near-infrared, at around 1400 and 1900 nm, due to vibrational transition in the O-H and H-O-H bonds (crystallisation water; Hunt et al., 1971) and a strong absorption band in the spectral range between 962 and 969 nm, due to electronic iron transition (Hunt and Salisbury, 1970; Baumgardner et al., 1985).

As expected, the 1400 and 1900 nm absorption bands are present in the reflectance spectra of iron hydroxides (Figure 5), including the akaganéite (Murad and Bishop, 2000). The absorption bands appearing between 962 and 969 nm can be, instead, basically related to the goethite (964 nm) and akaganéite (962 nm; Scheinost et al., 1988). In lepidocrocite and ferrihydrite spectra the position of the band is shifted toward higher wavelengths (976 and 1018 nm, respectively).

The Fe^{2+} synthetic gleys (Figure 7) also display a band between 659 and 664 nm, which may still be correlated to the presence of goethite (661 nm, in the reference spectrum; Figure 5). The spectra of pH 7.0 and pH 8.5 Fe^0 synthetic gleys (Figure 6) display two evident bands within the spectral ranges 958-967 nm and 658-673 nm, correlated to the presence of goethite and lepidocrocite (Figure 5).

Finally, both the Fe^0 (Figure 6) and Fe^{2+} synthetic gleys (Figure 7) show several bands below 650 nm, due to electronic iron transition. The identification of these large and shallow bands is, however, very difficult. The problem will be resolved, as we shall see better later in this paper, with the help of second derivative spectroscopy.

The information acquired through the visual inspection of reflectance spectra led to conclusions consistent with the results of the X-ray powder diffraction, previously discussed. In fact, the latter revealed the presence of goethite and akaganéite, in samples obtained from the Fe^{2+} synthetic gleys, and of magnetite and goethite, and subordinately of lepidocrocite, in Fe^0 synthetic gleys. In respect to what has been revealed by the X-ray diffraction, it has not been possible to diagnose the presence of hematite in the only sample of pH Fe^{2+} synthetic gleys that contained this oxide, probably because of its low concentration in the sample.

Analysis of colour

Found that, in accordance with the highest reflectance in the visible, of samples of the Fe^{2+} synthetic gleys appear lighter than those of Fe^0 synthetic gleys (data not shown), the variability of the colour of our experimental samples are well represented in the chromaticity diagram shown in Figure 8. This diagram, along with the values of chroma and hue (as polar coordinates) of the experimental samples, shows, as reference, group of samples of pure goethite, hematite, lepidocrocite and ferrihydrite (Schwertmann and Cornell, 2000) as well as the median values of the akaganéite (Schwertmann and Cornell, 2000) and the values of the only available sample of magnetite, computed from a spectrum of this oxide taken from the USGS spectral library (Grove et al., 1992).

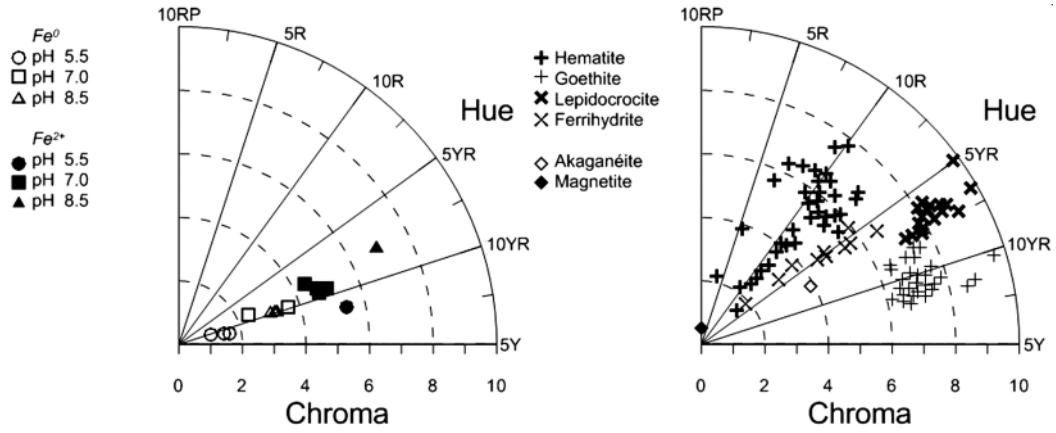

Figure 8. Distribution of samples of Fe^0 and Fe^{2+} synthetic gleys (left) compared with those of hematite, ferrihydrite, lepidocrocite and goethite (right) on the space defined Munsell chroma and hue (polar diagram of chromaticity).

From the analysis of Figure 8, it appears evident that our experimental synthetic gleys are distributed within a range of variability defined by a hue relatively narrow, centred at 10YR, and comprised between 7.5YR and 2.5Y. In particular, chroma increases as the number of oxidation and the pH of the preparation of synthetic gleys also increases. In essence, the distribution of chromaticity parameters of the experimental synthetic gleys fall within a range of variability defined, as lower limit, by the paradigm of magnetite (5R/0) and, as upper limit, by the paradigm of goethite (10YR/7), intersecting the paradigm of akaganéite (7.5YR/4).

This distribution is perfectly consistent with the results of XRPD, and shows how the different conditions of preparation of synthetic gleys directed the evolution of iron toward the phases of magnetite, present only in the Fe^0 synthetic gleys, and in larger amount in the samples prepared at acidic pH (Table 2), or those of akaganéite, present only in the Fe^{2+} synthetic gleys, and in larger amount in the samples prepared at neutral pH (Table 2). Besides, the phases of goethite are always represented, although in a greater amount in the Fe^{2+} synthetic gleys, with little dependence on the pH of preparation.

Indeed, the experimental data suggest that the presence of goethite unequivocally acts as a driver of the spectral response within the range of the observed variability. In fact, the position of each experimental sample is determined both by the presence of the characterising phase - that is, magnetite, for the Fe^0 synthetic gleys and akaganéite, for the Fe^{2+} synthetic gleys and the relative abundance of goethite in respect to that of each of these phases: as the relative content of goethite decreases, the chroma also decreases, moving toward the values of the pure phases such as magnetite and akaganéite; conversely, as the relative content of goethite increases, the value of chroma increases, thus moving toward the chromatic domain of that iron oxide. As a consequence, for a correct interpretation of chromaticity parameters, it is essential to take into account the co-presence of the different phases, which act as "attractors" of the position of a given sample within the chromaticity diagram.

Table 3. Position (P) and amplitude (A) of the absorption bands in the visible region, below 600 nm, of samples of Fe^0 and Fe^{2+} synthetic gleys.

Fe^0 - synthetic gleys

Sample	P	A	P	A	P	A	P	A	P	A
pH 5.5 (a)	-	-	416	0.74	-	-	488	0.19	521	0.82
pH 5.5 (b)	370	1.03	400	0.04	424	1.19	491	0.24	519	1.03
pH 5.5 (c)	394	0.23	-	-	421	1.63	489	1.56	520	1.04
pH 7.0 (a)	385	0.25	417	0.68	-	-	487	0.04	521	2.87
pH 7.0 (b)	366	1.65	414	1.54	-	-	486	0.31	519	3.23
pH 8.5 (a)	374	1.34	-	-	422	1.54	487	0.53	520	2.26
pH 8.5 (b)	362	0.42	-	-	421	1.44	487	0.47	521	2.33
pH 8.5 (c)	399	0.03	-	-	-	1.31	487	0.41	520	2.32
Median value	*374*		*414*		*422*		*487*		*520*	

Fe^{2+}- synthetic gleys

Sample	P	A	P	A	P	A	P	A	P	A
pH 5.5	364	2.59		-	421	4.96	492	3.50		-
pH 7.0 (a)	374	0.95		-	420	3.96	493	2.86		-
pH 7.0 (b)	371	1.39	419	3.14		-	493	2.55		-
pH 7.0 (c)	387	0.04		-	420	3.85	494	2.88		-
pH 7.0 (d)	366	2.87	418	3.74		-	493	2.89		-
pH 8.5	375	1.58		-	422	3.66	489	0.91	564	2.84
Median value	*373*		*419*		*421*		*493*		*564*	

a, b, c, d: subsamples.

In other words, the position along the hue vector for the different intensities of saturation is determined by the relative proportions of the individual phases in the sample. This implies that, for a particular domain of hue, the expression of the chroma becomes discriminant for predicting not only the presence but also the relative abundance of a specific phase.

Derivative spectroscopy

The analysis of second derivative spectra allowed the identification of five main absorption bands in the visible region (Table 3), below 650 nm, determined by electronic transitions in the crystal structures of different types of iron oxides and hydroxides, linked to the evolution of the experimental Fe^0 and Fe^{2+} synthetic gleys under investigation.

All samples extracted from the Fe^0 synthetic gleys (Table 3) show an absorption band falling in a range of wavelengths between 486 and 491 nm, with a median value of 487 nm. Scheinost et al. (1998), working on synthetic iron oxides, have attributed to the goethite a band between 479 and 493 nm, with a median value of 488 nm, and to the lepidocrocite a band between 485 and 490 nm, with a median of 488 nm. Accordingly, we can attribute to both goethite and lepidocrocite the band located around 487 nm in samples of Fe^0.

Other bands are present below the 450 nm, but not in all of the samples of Fe^0. In agreement with the existing literature (Scheinost et al., 1998), these bands fall within, and overlapping, intervals of absorption of different iron oxides. Therefore, their attribution to specific iron oxides is quite difficult, if not impossible.

Samples of Fe^0 synthetic gleys also show a band around a median value of 520 nm, between the extreme values of 519 and 521 nm. The analysis of the literature would lead to attribute this band to electronic transition processes in the hematite. In effect, the position of the absorption band of this iron oxide is more precisely located at longer wavelengths, between 527 and 565 nm, with a median value of 531 nm (Scheinost et al., 1998). However, a band at 524 nm, the closest to that observed in Fe^0 synthetic gleys, has been found in the only available spectrum of magnetite (Figure 5). Therefore, it is reasonable to attribute to the magnetite the band found around 520 nm in samples of Fe^0.

Contrary to expectations, the amplitude of the 520 nm band decreases, rather than increases, as the amount of magnetite increases. On the other hand, it increases with increasing goethite content. This result is somewhat surprising if one thinks that, according to the available knowledge (Scheinost et al., 1998; Torrent and Barrón, 2002), goethite should not determine the absorption bands between 500 and 600 nm. In light of the experimental data, one could argue that the goethite "interferes" with the absorption of magnetite at 520 nm. This aspect is not clear at the moment; therefore, it needs to be specifically investigated in the future.

The samples produced from the Fe^{2+} synthetic gleys (Table 3) show a band centred at around a median value of 493 nm. This wavelength corresponds substantially to the median value (492 nm) of a very narrow variation range (490-493 nm), found by Scheinost et al. (1998) in samples of synthetic akaganéite. It is also the maximum value of the variation (497-493 nm) of goethite (Scheinost et al., 1998). Therefore, it is plausible to attribute the band at 492 nm to the presence of akaganéite and, subordinately, of goethite.

The above findings further confirm the consistency of spectrometric data with those obtained by conventional XRPD analysis.

Conclusions

Visible-near infrared reflectance spectroscopy is an innovative and promising method that is very effective for the characterization of the soil gley forms. As a matter of fact, such method foretells great advantages: (i) consistent supplement to canonical XRPD analysis; (ii) evaluation, in gleyed soils horizons, of different iron forms undetectable by conventional Munsell colour charts, as well as impossible to separately pick up and analyse; (iii) accuracy and precision in comparison to visual colour analysis; (iv) reliability and (v) time and money saving.

The results obtained appear to be as original as significant, and highly stimulating for further investigation dealing with iron synthetic gleys obtained by Fe^{3+} and Fe^0 in alkaline environments, the modulation of drying and exposure to oxygen, and the setting up of field procedures.

Acknowledgements

We wish to thank Maurizio Tosca, for his valuable help in the realisation of spectroscopic measurements. The authors are grateful to two anonymous referees whose suggestions definitely improved the paper. We gratefully acknowledge the scientific director of Periodico di Mineralogia Antonio Gianfagna and the editorial assistant Giovanni B. Andreozzi for the careful handling of the manuscript. A special thank is also due to the Associated editors Maurizio de Gennaro, Maria Rosaria Ghiara and Giuseppina Balassone.

References

Barrón V. and Torrent J. (1984) - Influence of aluminum substitution on the color of synthetic hematites. *Clays*

and Clay minerals, 32, 157-158.

Baumgardner M.F., Silva L.F., Biehl L.L. and Stoner R. (1985) - Reflectance properties of soils. *Advances in Agronomy*, 38, 1-44.

Burns R.G. (1993) - Remote-Sensing composition of planetary surfaces: applications of reflectance spectra. In: Mineralogical Applications of Crystal Field Theory, 2nd Ed, Cambridge Topics in Mineral Physics and Chemistry No. 5, Cambridge University Press: Cambridge, United Kingdom, 396-427.

Calabrò G. and Tosca M. (2009) - SpecPro release a 2.95, Software per il processing di dati spettroradiometrici. Report CNR-ISAFoM.

Chadburn B.P. (1982) - Derivative spectroscopy in the laboratory: advantages and trading rules. *Proceedings Analytical Division Chemical Society*, 54, 42-43.

CIE, Commission Internationale de l'Eclairage (1978) - Recommendations on uniform color spaces, color difference and psychometric color terms. Supplement No. 2. Publ. No. 15. Colorimetry, CIE 1971, Paris.

Clark R.N. (1999) - Spectroscopy of rocks and minerals, and principles of spectroscopy. http://speclab.cr.usgs.gov.

Clark R.N., King T.V.V., Klejwa M. and Swayze G.A. (1990) - High spectral resolution reflectance spectroscopy of minerals. *Journal of Geophysical Research*, 95, 12653-12680.

Cornell R.M. and Schwertmann U. (1996) - The iron oxides. Structure, properties, reactions, occurrence and uses. VCH Publishers, New York, 573 pp.

Cornell R.M. and Schwertmann U. (2003) - The Iron Oxides Structure, Properties, Reactions, Occurences and Uses. WILEY-VCH Verlag GmbH & Co. KGaA,Weinheim, 664 pp.

Drury S.A. (1993) - Image interpretation in geology. Chapman & Hall, London, 173 pp.

Escadafal R. (1993) - Remote sensing of soil color: principles and applications. *Remote Sensing Reviews*, 7, 261-279.

Escadafal R. (1994) - Soil spectral properties and their relationships with environmental parameters - Examples from arid regions. In: Hill J., Mégier J., Eds, "Imaging Spectrometry - a tool for Environmental Observations". Kluwer Academic Publishers, Amsterdam, 71-87.

Grove C.I., Hook S.J. and Paylor E.D. (1992) - Laboratory reflectance spectra of 160 minerals, 0.4 to 2.5 micrometers. JPL-Public. 92-2, Pasadena, California, 406 pp.

Huguenin R.L. and Jones J.L. (1986) - Intelligent information extraction from reflectance spectra: absorption band positions. *Journal of Geophysical Research*, 91, 9585-9598.

Hunt G.R. (1980) - Electromagnetic radiation: the communications link in remote sensing. In: Remote sensing in geology, (B.S. Siegal and A.R. Gillespie Eds), Wiley, New York, 5-45.

Hunt G.R. and Salisbury J.W. (1970) - Visible and near-infrared spectra of minerals and rocks. I. Silicate minerals. *Modern Geology*, 1, 283-300.

Hunt G.R., Salisbury J.W. and Lenhoff C.J. (1971) - Visible and near-infrared spectra of minerals and rocks. III. Oxides and hydroxides. *Modern Geology* 2, 195-205.

Irons J.R., Weismiller R.A. and Petersen G.W. (1989) - Soil reflectance, In: Theory and Applications of optical remote sensing; G. Asrar, Ed.; Wiley: New York, 1989, 66-106.

IUSS-ISRIC-FAO (2006) - World Reference Base for Soil Resources. 2nd edition. World Soil Resources Reports No. 103. FAO, Rome.

Judd D.B. and Wyszecki G. (1975) - Color in Business, Science and Industry (3rd ed.). New York, Wiley.

Kosmas C.S., Curi N., Bryant R.B. and Franzmeier D.P. (1984) - Characterization of iron oxide minerals by second-derivative visible spectroscopy. *Soil Science Society of American Journal*, 48, 401-405.

Kosmas C.S., Franzmeier D.P. and Schulze D.G. (1986) - Relationship among derivative spectroscopy, colour, crystallite dimensions, and Al substitution of synthetic goethites and hematite. *Clays and Clay Minerals*, 6, 625-634.

Leone A.P. (2000) - Bi-directional reflectance spectroscopy of Fe-oxides minerals in Mediterranean Terra Rossa soils: a methodological approach. *Agricoltura Mediterranea*, 130, 144-154.

Leone A.P. and Escadafal R. (2001) - Statistical analysis of soil colour and spectroradiometric data for hyperspectral remote sensing of soil properties (example in a southern Italy Mediterranean ecosystem). *International Journal of Remote Sensing*, 12, 2311-2328.

Loercher G. (1996) - Investigation of data processing model for integrating hyperspectral data sets into GIS. In: Proc. Second International Airborne Remote Sensing Conference and Exhibition, San Francisco, California, 24-27 June 1996, 3, 112-117.

Malengreau N., Muller J.P. and Calsa G. (1994) - Fe-speciation in kaolins: a diffuse reflectance study. *Clays and Clay Minerals*, 42, 137-147.

Manceau A. and Drits V.A. (1993) - Local structure of ferrihydrite and feroxyhite by EXAFS spectroscopy. *Clay Minerals*, 28, 165-184.

Milton E.J., Rollin E.M. and Emry D.R. (1995) - Advances in field spectroscopy. In: Advances in environmental remote sensing (F.M. Danson and S.E. Plummer, Eds.), John Wiley and Sons, Chichester, 9-32.

Miyahara M. and YoshidaY. (1988) - Mathematical transform of R, G, B color data to Munsell H, V, C color data. In: Huang, T.R. (Ed.), SPIE Conference on Visual Communications and Image Processing '88, Cambridge, MA, 1001, 650-657.

Morris R.V., Agresti D.G., Lauer H.V., Newcomb J.A., Shelfer T.D. and Murali A.V. (1989) - Evidence for pigmentary hematite on Mars based on optical, magnetic, and Mössbauer studies of supermagnetic (nanocristalline) hematite. *Journal of Geophysical Research*, 94, 2760-2778.

Murad E. and Bishop J.L. (2000) - The infrared spectrum of synthetic akaganéite, ß-FeOOH. *American Mineralogist*, 85, (5-6), 716-721.

O'Havers T.C. (1982) - Derivative spectroscopy and its applications in analysis: derivative spectroscopy: theoretical aspects. Plenary Lecture, *Analytical Proceedings*, 54, 22-28.

O'Havers T.C. and Green G.L. (1976) - Numerical error analysis of derivative spectrometry for quantitative analysis of mixtures. *Analytical Chemistry*, 48, 312-318.

Savitzky A. and Golay M.J.E. (1964) - Smoothing and differentiation of data by simplified least squares procedures. *Analytical Chemistry*, 36 (8), 1627-1639.

Scheinost A.C. (2004) - Metal oxides. In: Hillel D. (ed) Encyclopedia of soils in the environments, Elsevier, 428-438.

Scheinost A.C. (2000) - Methods of characterization. In: U. Schwertmann and R.M. Cornell, Iron Oxides in the laboratory. Preparation and characterization. Wiley-VCH, 27-54.

Scheinost A.C. and Schwertmann U. (1999) - Color identification of iron oxides and hydroxysulfates: use and limitations. *Soil Science Society of American Journal*, 63, 1463-1471.

Scheinost A.C., Chavernas A., Barrón V. and Torrent J. (1998) - Use and limitations of second-derivative diffuse reflectance spectroscopy in the visible to near-infrared range to identify and quantify Fe Oxide minerals in soils. *Clays and Clay Minerals*, 5, 528-536.

Schoeneberger P.J., Wysocki D.A., Benham E.C. and Broderson W.D. (editors) (2002) - Field book for describing and sampling soils, Version 2.0. Natural Resources Conservation Service, National Soil Survey Center, Lincoln, NE.

Schwertmann U. (2008) - Iron Oxides, In: Encyclopedia of soil science. Ward Chesworth Ed., Springer, Dordrecht, The Netherlands, 363- 369.

Schwertmann U. and Cornell R.M. (2000) - Iron Oxides in the laboratory. Preparation and characterisation. Wiley-VCH, 27-54.

Shepherd K.D. and Walsh M.G. (2006) - Diffuse Reflectance Spectroscopy for Rapid Soil Analysis. Encyclopedia of Soil Science, Taylor & Francis, 480-484.

Sherman D.M. and Waite T.D. (1985) - Electronic spectra of Fe^{3+} oxides and oxides hydroxides in the near infrared to ultraviolet. *American Mineralogist*, 70, 1262-1269.

Singer R.B. (1982) - Spectral evidence for mineralogy of high-albedo soils and dust of Mars. *Journal of Geophysical Research*, 87, 10159-10168.

SSSA - Soil Science Society of America (2008) - Glossary of Soil Science Terms 2008. Soil Science Society of America, Inc., Madison, WI, 93 pp.

Stenberg B., Viscarra-Rossel R.A., Mouazen A.M. and Wetterlind J. (2010) - Visible and near infrared spectroscopy in soils science. *Advances in Agronomy*, 107, 163-215.

Taylor K.J. and Konhauser K.O. (2011) - Iron in Earth surface Systems: a major player in chemical and biological processes. *Elements*, 7(2), 83-88.

Torrent J. (1995) - Genesis and properties of the soils of the Mediterranean regions. Università degli Studi di Napoli Federico II, Dipartimento di Scienze Chimico-Agrarie. Arti Grafiche Licenziato, Napoli. 111 pp.

Torrent J. and Barrón V. (1993) - Laboratory measurement of soil color: theory and practice. In: Soil Color (J.M. Bigham and E.J. Ciolkosz eds.). *SSSA Special Publication*, 31, 21-33.

Torrent J. and Barrón V. (2002) - Diffuse reflectance spectroscopy of iron oxides. Encyclopedia of Surface and Colloid Science, 1438-1446.

Torrent J. and Schwertmann U. (1987) - Influence of

hematite on the color of red beds. *Journal of Sedimentary Petrology*, 57, 682-686.

Tsai F. and Philpot W. (1998) - Derivative analysis of hyperspectral data. *Remote Sensing Environment*, 66, 41-51.

USDA-NRCS (1999) - Soil Survey Staff - United States Department of Agriculture. Soil Taxonomy, A Basic System of Soil Classification for Making and Interpreting Soil Surveys, 2nd ed., Agriculture Handbook n. 436, U.S.D.A., Natural Resources Conservation Service, NY.

Valeriano M.M., Epiphanio J.C.N., Formaggio A.R. and Oliveira J.B. (1995) - Bi-directional reflectance factor of 14 soil classes from Brazil. *International Journal of Remote Sensing*, 1, 113-128.

Viscarra- Rossel R.A., Minasny B., Roudier P. and McBratney A.B. (2006) - Colour space models for soil science, *Geoderma*, 133, 320-337.

Vodyanitskii Yu. N. (2010) - Iron Hydroxides in Soils: A Review of Publications. *Eurasian Soil Science*, 43/11, 1244-1254.

Wyszecki G. and Stiles W.S. (1982) - Color science: concepts and methods, quantitative data and formulae. John Wiley and Sons, New York, 950 pp.

Yli-Halla M., Mokma D.L., Wilding L.P. and Drees L.R. (2006) - Formation of a cultivated Spodosol in East-Central Finland. *Agricultural and Food Science*, 15, 12-22.

Submitted, July 2011 - Accepted, November 2011